Published in final edited form as:
Nature. ; 474(7350): 216–219. doi:10.1038/nature10160.

In vivo imaging of Tregs providing immune privilege to the hematopoietic stem cell niche

Joji Fujisaki[1,2], **Juwell Wu**[1,2,3], **Alicia L. Carlson**[1], **Lev Silberstein**[2,4], **Prabhakar Putheti**[5], **Rafael Larocca**[5], **Wenda Gao**[5], **Toshiki I. Saito**[6], **Cristina Lo Celso**[2,4], **Hitoshi Tsuyuzaki**[7], **Tatsuyuki Sato**[7], **Daniel Côté**[8], **Megan Sykes**[6], **Terry B. Strom**[5], **David T. Scadden**[2,4], and **Charles P. Lin**[1,2]

[1]Advanced Microscopy Program, Center for Systems Biology and Wellman Center for Photomedicine, Massachusetts General Hospital, Harvard Medical School, CPZN 8238, 185 Cambridge Street, Boston, MA 02114, USA

[2]Harvard Stem Cell Institute, 42 Church Street, Cambridge, MA 02138, USA

[3]Harvard-MIT Division of Health Sciences and Technology, 77 Massachusetts Avenue, E25-519, Cambridge, MA 02139, USA

[4]Center for Regenerative Medicine, Massachusetts General Hospital, 185 Cambridge Street, Boston, MA 02114, USA

[5]Transplantation Institute and Department of Medicine, Beth Israel Deaconess Medical Center, Boston, MA 02215, USA

[6]Bone Marrow Transplantation Section, Transplantation Biology Research Center, Massachusetts General Hospital, MGH-East, Bldg.149-5102 13th Street, Boston, MA 02129 USA.

[7]Faculty of Medicine, The University of Tokyo, 7-3-1 Hongo, Bunkyo-ku, Tokyo, 113-0033, Japan

[8]Département de Physique, Génie Physique et Optique & Centre de Recherche Université Laval Robert Giffard Québec City, Québec, G1J 2G3 Canada

Abstract

Stem cells reside in a specialized regulatory microenvironment or niche[1,2], where they receive appropriate support for maintaining self-renewal and multi-lineage differentiation capacity[1-3]. The niche may also protect stem cells from environmental insults[3] including cytotoxic chemotherapy and perhaps pathogenic immunity[4]. The testis, hair follicle, and placenta are all sites of residence for stem cells and are immune suppressive environments, called immune privileged (IP) sites, where multiple mechanisms conspire to prevent immune attack, even enabling prolonged survival of foreign allografts without immunosuppression (IS)[4]. We sought to determine if somatic stem cell niches more broadly are IP sites by examining the hematopoietic stem/progenitor cell (HSPC) niche[1,2,5-7] in the bone marrow (BM), a site where immune reactivity exists[8,9]. We observed persistence of allo-HSPCs in non-irradiated recipients for 30 days without IS with the same survival frequency compared to syngeneic HSPCs. These HSPCs were lost after the depletion of FoxP3 regulatory T cells (Tregs). High resolution *in vivo* imaging over time demonstrated marked co-localization of HSPCs with Tregs that accumulated on the endosteal surface in the calvarial and trabecular BM. Tregs appear to participate in creating a localized zone where HSPCs reside and

Correspondence should be addressed to J.F. (jfujisaki@partners.org) and C. P. L. (lin@helix.mgh.harvard.edu)..

Category
Hematology, Immunology, Stem cell biology, Stem cell transplantation, Imaging

where Tregs are necessary for allo-HSPC persistence. In addition to processes supporting stem cell function, the niche will provide a relative sanctuary from immune attack.

Keywords

Immune privilege; IP; HSC niche; stem cell niche; bone marrow; regulatory T cell; Treg; FoxP3; *in vivo* microscopy; imaging

---

Despite rapid advances in our understanding of adult stem cell biology, the immunological attributes of somatic stem cell niches have remained largely unexplored. We hypothesized that the HSPC niche within the BM[6,7] is an IP site based on the observation that human BM contains higher frequency of CD4+CD25+FoxP3+ regulatory T cells (Tregs) than other secondary lymphoid organs[10]. We used intravital microscopy (IVM)[11-13] to visualize the localization of Tregs and transplanted HSPCs within the BM of live animals.

Prolonged survival of allografts or xenografts without IS was a criterion used by Peter Medawar to demonstrate IP in sites such as the testis, the eye and the brain[4]. To test if the HSPC niche is an IP site that meets the above criterion, we first examined if allo-HSPCs transplanted into non-irradiated recipients would survive *without any IS*. C57BL/6 (B6) Ckit +Sca1+Lin− (KSL) HSPCs labelled by a membrane dye, DiD, were injected into non-irradiated allogeneic BALB/c mice or syngeneic B6 mice. Using IVM, we imaged identical volumes of the recipient skull BM[12,13] on day 30 (Supplementary Fig. 1). Surprisingly, the numbers of surviving KSL cells in the skull BM were comparable in the syngeneic and allogeneic recipients (Fig. 1a-b and Supplementary Fig. 1). Approximately 90% of the donor cells in both recipients were found near the endosteal surface, a location that has been identified as an HSPC niche[6,7] (Fig. 1c). The majority of KSL cells in both syngeneic and allogeneic groups retained high levels of DiD, indicating that HSPCs did not undergo extensive proliferation. B6 derived cells were not detected in the blood by flow cytometry (data not shown).

Phenotypic analysis showed that surviving donor cells contained a significant fraction of B6 KSL HSPCs and CD150+CD48−KSL hematopoietic stem cells (HSCs) (Supplementary Fig. 2). To determine if they contain functional HSCs, we performed secondary transplant of BALB/c recipient BM into sub-lethally irradiated B6 mice and confirmed long-term multi-lineage reconstitution derived from first donor cells (Supplementary Fig. 3 and Supplementary Table). These results indicate that HSCs with long-term repopulating potential persisted in non-irradiated allogeneic recipients without IS.

Reciprocal transplant of BALB/c CD150+CD48−Lin− HSPCs into B6 mice shows that allo-HSPCs can survive in non-irradiated mice regardless of the combination of strains used as donors and recipients (Supplementary Fig. 4).

To explore the possibility that immune ignorance may be the cause of the prolonged survival of allo-HSPCs in non-irradiated recipients, we first examined MHC class I antigen expression and found higher levels of H2-Kb on B6 KSL cells than on spleen CD19+ B cells (data not shown)[14]. To address the possibility that transplantation of KSL cells alone without differentiated cells may fail to evoke a potent allogeneic immune response, we transplanted DiD-labelled KSL cells (5×10^4 /mouse) alone or with non-labelled B6 whole BM cells (5×10^7 /mouse) into non-irradiated BALB/c recipients and detected comparable numbers of surviving DiD-positive B6 cells with or without co-transplantation of whole BM cells (Fig. 1b). The inability of the host to reject these cells is therefore not likely due to immune ignorance, but may reflect active immune regulation.

We next tested if prolonged survival of allogeneic cells in non-irradiated recipients is unique to HSPCs. We simultaneously injected B6 KSL HSPCs and B6 Lin+ differentiated cells labelled with two different dyes DiD and DiI into non-irradiated BALB/c or B6 mice. *In vivo* imaging of the skull BMs of the allogeneic BALB/c recipients 2 days later showed the presence of both DiI-labelled B6 Lin+ cells and DiD-labelled B6 KSL cells (Fig. 1d), but in contrast to the KSL cells, the Lin+ cells were distributed farther away from the endosteal surface (Supplementary Fig. 5). Notably, on day 7, Lin+ cells were virtually undetectable, while the HSPCs persisted (Fig. 1d). In the syngeneic B6 recipients, both populations survived on day 7 (Fig. 1d).

Prolonged survival of allo-HSPCs in non-irradiated recipients is consistent with Peter Medawar's observation of prolonged survival of transplanted allogeneic/xenogeneic grafts in other IP sites[4], supporting our hypothesis that the HSPC niche also has IP mechanisms that shield the transplanted allo-HSPCs, but not their differentiated counterpart, from allogeneic immune response.

Next, we examined the relevance of Tregs to IP in the HSPC niche. We confirmed that the frequency of FoxP3 Tregs in CD4 T cells is higher in the BM (23%) than in the spleen (13%) and lymph nodes (13%) (data not shown). As the trafficking of Tregs to the BM critically depends on the stem cell chemo-attractant, SDF-1[10], which is expressed at high levels by cellular components of the HSPC niche[13,15-17], we hypothesized that Tregs will accumulate in the HSPC niche and render it immune suppressive. *In vivo* 3D imaging of the intact skull and mechanically thinned proximal tibia of FoxP3−GFP mice showed that 58% (203/350) and 72% (137/191) of Tregs were within 15 μm of the endosteal surface (Fig. 2a-b). Preferential localization of Tregs on the endosteal surface was also confirmed by analysis of 2D histological sections (Fig. 2b and Supplementary Fig. 6).

Next, we examined the relative spatial distribution of Tregs and transplanted HSPCs by *in vivo* 3D imaging. Remarkably, >80% of the DiD-labelled B6 KSL cells homed within 20 μm of Tregs on the endosteal surface 24 hours after intravenous injection into FoxP3−GFP B6 mice (Fig. 2a, c). In contrast, Lin+ differentiated cells were much less likely to home close to Tregs (Fig. 2c). Close proximity of transplanted KSL cells and Tregs on the endosteal surface was confirmed by histological analysis of the tibia and femur trabecular BM (Supplementary Fig. 6). We also visualized the quiescent HSCs after administering the chemotherapy drug 5-fluorouracil (5-FU), which selectively killed dividing cells. *In vivo* imaging of the skull BM 48 hours after 5-FU treatment showed that 82% (36/44) of the 5-FU resistant DiD-labelled KSL cells were within 20 μm of the FoxP3−GFP Tregs (Fig. 2d), forming clusters with Tregs on the endosteal surface. Similarly, Tregs accumulated around allo-HSPCs that survived on the endosteal surface of the skull BM and trabecular BM of long bones in non-irradiated mice for 30 days without IS (Fig. 2e, Supplementary Fig. 7). In cortical BM of long bones, only 32% (38/120) of allo-HSPCs and 11% (15/137) of Tregs were within 15 μm of the endosteal surface, but proximity of Tregs to allo-HSPCs was still noted irrespective of their distance to the endosteal surface (Fig. 2b and Supplementary Fig. 7).

To examine whether Tregs play a critical role in providing IP to the HSPC niche, we examined if Treg depletion resulted in the rejection of allo-HSPCs without IS. Using FoxP3−GFP diphtheria toxin receptor (DTR) mice, whose Tregs express DTR and can be specifically depleted by diphtheria toxin (DT) treatment (data not shown), we observed a 70% reduction in the number of surviving donor cells in DT treated vs. control vehicle treated recipients (Fig. 3a). Treg depletion by anti-CD25 antibody also led to a 90% reduction in the number of surviving donor cells compared with control antibody treated recipients (Supplementary Fig. 8). Quantitative real-time PCR (qt-RT-PCR) analysis of

CD4+FoxP3− T cells and CD8 T cells isolated from the BM showed increased levels of TNF-α, and IL-4 expression in DT treated vs. control B6N9 FoxP3−GFP DTR mice transplanted with BALB/c HSPCs (Supplementary Fig. 9). Together these results indicate that Tregs critically provide the HSPC niche with IP and that Treg-mediated suppression of BM CD4 and CD8 T cell activation is at least in part responsible for the survival of allo-HSPCs in non-irradiated hosts without IS.

We also performed qt-RT-PCR analysis of Tregs from B6 FoxP3−GFP recipients 6 days after transplantation of BALB/c CD150+CD48−Lin−HSPCs without IS. TGF-β mRNA level in BM FoxP3 Tregs was four-fold higher compared with spleen Tregs of transplanted recipients, but this level was comparable to that of BM Tregs of non-transplanted recipients (Fig. 3b). In contrast, IL-10 mRNA level in BM Tregs of transplanted recipients was significantly higher compared with control BM Tregs without transplant, and was also significantly higher compared with spleen Tregs of transplanted mice (Fig. 3b). Increase of IL-10 expression at the protein level in BM FoxP3 Tregs was also confirmed using FACS analysis after intracellular staining (Fig. 3c). Consistent with these findings, anti-IL-10R antibody treatment led to ~90% reduction of the number of surviving allo-HSPCs compared with control IgG antibody treatment, while anti-TGF-β antibody treatment did not have a significant effect on the number of donor cells (Fig. 3d).

To test the specific role of IL-10 in Tregs, we used as transplant recipients non-irradiated B6 RAG2 knockout (KO) mice reconstituted one day earlier with B6 IL-10 KO CD4+CD25+ Tregs or B6 wild-type CD4+CD25+ Tregs together with B6 wild-type CD4+CD25− T cells. The numbers of DiD-labelled BALB/c HSPCs surviving for 7 days in the recipients with IL-10 KO Tregs were dramatically lower than that in control recipients with wt CD4+CD25+ T cells (Fig. 3e). Together, the data indicate that IL-10 from Tregs is critical for Treg-mediated IP protection of allo-HSPCs in non-irradiated recipients.

We show here that in anatomic locations where immune activity is otherwise known to occur[8,9], discrete sites of IP may exist and contribute to a somatic stem cell niche. Prolonged survival of allo-HSPCs without IS is surprising and appears contrary to the clinical experience that indicates strong IS is required to prevent rejection in allogeneic BM transplantation[18]. We propose that our data may not be in conflict with that well-defined experience since we are observing events at the level of the HSPC in non-irradiated hosts, while the clinical transplant measure of engraftment is mature cell chimerism. In transplantation without IS, mature cells are susceptible to immune attack and low levels of HSPC chimerism in the relative absence of proliferation may go undetectable by conventional methods.

Tregs accumulate in the HSPC niche and may provide the HSPC niche with IP mechanisms, enabling transplanted allo-HSPCs to escape from allogeneic rejection. IP mechanisms of the HSPC niche will shield endogenous HSPCs from autoimmunity or excessive inflammation, and will even help malignant cells evade host immunity. This work raises the possibility of niches in other tissues serving as IP sites.

Methods

Mouse

FoxP3 GFP knock-in mice (C57B/6L or BALB/c background) were provided by Terry Strom's laboratory. FoxP3−GFP diphtheria toxin receptor (DTR) mice were provided by Rudensky's laboratory. C57B/6L mice, BALB/c mice and IL-10 KO mice were purchased from Jackson laboratory. RAG2 KO mice were purchased from Taconic, Inc. All animal

experiments were performed in compliance with institutional guidelines and approved by the Subcommittee on Research Animal Care (SRAC) at Massachusetts General Hospital.

Hematopoietic stem cell isolation

Whole bone marrow was obtained from C57B/6L mice or BALB/c mice by crushing the femur, tibia, iliac, humerus, and vertebral bones. Cells were pooled and washed with PBS, then incubated in a lineage cocktail consisting of biotinylated B220, Mac1, GR-1, CD3a, CD8a, CD4 and Ter119 antibodies. After washing, cells were incubated with MACS-SA beads (Miltenyi) per manufacturer's protocol, washed again, then separated on a LD depletion column in a MidiMACS separation unit in order to remove lineage-specific cell populations. Lineage-negative cells from B6 mice were then stained with Ckit-APC and Sca1-PE antibodies. Lineage-negative cells from BALB/c mice were stained with CD48−APC and CD150−PE antibodies. Subsequently, Sca1+Ckit+Lin− cells or CD150+CD48−Lin− cells were isolated by FACS sorting machine (BD FACSAria). Cells were then stained with DiD and injected into recipient mice for intravital confocal microscopy.

Fluorescence cell labelling

Sca1+Ckit+Lin− cells, Lin+ cells, and CD150+CD48−Lin− cells were fluorescently labelled by incubation with the dialkylcarbocyanine membrane dyes, “DiD” or “DiI”. Cells in culture media were incubated with 10 μM dye for 30 minutes at 37°C. Cells were then centrifuged and the pellet washed in PBS × 3 prior to injection in animals.

In vivo imaging

In vivo imaging of the bone marrow through the intact skull bone of live mice was first demonstrated by von Andrian and coworkers[11]. Here we used a video-rate laser scanning hybrid confocal/two-photon microscope that is specifically designed and optimized for live animal imaging[12,13]. A polygon-based scanning engine allows simultaneous multi-channel image acquisition at video rate (30 frames per second), a feature that is particularly useful for imaging moving objects. Fast scanning speed, together with a precision computer-controlled xyz stage, also facilitate surveying large tissue volumes in 3D and searching for rare cells in the BM.

The mice were anesthetized with intra-peritoneal injection of ketamine/xylazine, and a small incision was made in the scalp to expose the underlying skull. The skull bone was kept intact. Second harmonic microscopy was used to visualize the bone and to identify the major anatomical landmarks such as the central vein and the coronal suture. Bone is rich in type-1 collagen, which was imaged by second harmonic generation using 840 nm excitation and 420 nm detection. Using the crossing of the central vein and coronal sutures as landmarks, we imaged identical areas of the skull (~1650 μm × 2310 μm) encompassing most of the parasagittal BM cavities[12,13]. The maximum imaging depth was approximately 150 μm below the outer bone surface, allowing us to penetrate between 40 and 60% of bone marrow cavity space in over 75% of our measurements[12]. DiD signal was excited with a 638 nm helium-neon laser (Radius, Coherent Inc., Santa Clara, CA) and detected with a photomultiplier tube through a 695+/−27.5 nm bandpass filter (Omega Optical, Brattleboro, VT). GFP signal was excited with a 491 nm solid state laser (Dual Calypso, Cobolt AB, Stockholm, Sweden) and detected with a photomultiplier tube through a 528+/−19 nm bandpass filter (Semrock, Rochester, NY). Second harmonic generation signals from the bone were excited with an 840 nm Ti: sapphire laser (Spectra Physics, Tucson, AZ) and detected with a photomultiplier tube through a 435+/−20 nm bandpass filter (Semrock, Rochester, NY). Each image consisted of 30 frames averaged together. Imaging duration per mouse was approximately 2 hours.

For imaging the tibia BM, the outer skin was removed from the leg and tendons around the joints severed to detach adjoining muscles. The saphenous and medial marginal vessels were kept intact. Upon exposure of the tibia, the medial bone surface was then gently polished with 400 grit silicon carbide wet grinding paper (Struers, Cleveland, OH) while irrigated with PBS and viewed with a surgical microscope until the fine structures of the trabecular bone became visible under the thinned cortical bone. The area was cleaned with a PBS flush and imaged using the same setup as described above for imaging the skull BM. Maximal imaging depth is approximately 150 μm below the bone surface.

Histological analysis

Femurs and tibias were fixed in 4% paraformaldehyde for 4 hours at room temperature, cryoprotected in 30% sucrose for 2-3 hours, immersed in OCT compound (Sakura) and frozen in liquid nitrogen in the horizontal orientation. Thick frozen sections of undecalcified bone were obtained, whereby a layer of compact bone was removed from the top and the bottom of the specimen, leaving both sides of the bone marrow cavity accessible for imaging. The specimens were subsequently thawed, washed in PBS, embedded in agarose and imaged using the same setup as described above.

Image processing and analysis

Image processing and HSPC-microenvironment distance measurements were obtained using Image J as described in the previous paper[12]. A two-tailed t-test was applied in the two-group analysis. P values ≤ 0.05 were considered statistically significant. In the three and four group comparison, we performed one-way analysis of variance followed by an analysis of the three pairwise differences of interest using Bonferroni correction so that P values $\leq 0.05/3$ were considered statistically significant.

Flow cytometry analysis of transplanted donor HSPCs

BM cells were isolated from non-irradiated BALB/c mice 30 days after transplantation with B6 KSL cells (1×10^5 cells/mouse), depleted of Lin+ cells using EasySep (StemCell Technologies). Cells were subsequently stained with PE-H2Kb, APC-CD48, APC-Cy7-Ckit, Pacific Blue-Sca1, Pacific Orange-Streptavidin, PE-Cy7-CD150 antibodies. Cells were analyzed by FACS (BD FACSAria) with Flowjo software.

Secondary transplantation

BM cells were isolated from non-irradiated BALB/c mice (CD45.2) 30 days after transplantation with B6 KSL cells (CD45.2) (5×10^4 cells/mouse), depleted of CD4 and CD8 T cells, and intravenously transplanted into 7.0 Gy, or 8.4 Gy-irradiated B6 SJL mice (CD45.1). 30 days or 240 days after secondary transplantation, flow cytometry analysis of peripheral blood cells was performed following the staining of cells by PE-Cy5.5 conjugated CD45.2 antibody, PE conjugated H2Kb, and APC conjugated CD3, B220, CD11b, or Gr1 antibodies (all from BD Bioscience). Cells were analyzed by FACS machine (BD FACSAria). The data were analyzed by Flowjo.

Flow cytometry analysis of FoxP3−GFP Tregs

Whole bone marrow cells, spleen cells, and lymph node cells were isolated from FoxP3−GFP mice and stained with anti-CD4, CD25, NK1.1 antibodies (eBioscience). Intracellular staining for IL-10 was performed according to the manufacture's protocol (eBioscience).

5-FU treatment

8-week-old mice were injected with 5×10^4 million/mouse KSL HSPCs labelled by DiD. 24 hours later, the skull bone marrow was imaged by IVM. At the completion of the initial imaging session, the skull was flushed with sterile saline, and the scalp skin flaps were sewn closed using 5-0 non-absorbable nylon sutures. Mice were injected with 5-FU (250 mg/kg body weight, Sigma) intravenously (i.v.)[3]. 48 hours after 5-FU treatment[3], sutures were removed, and the area flushed and swabbed with sterile saline for subsequent skull bone marrow imaging.

DT treatment

Non-irradiated B6N9 FoxP3−GFP DTR mice were transplanted with DiD-labelled BALB/c CD150+CD48−Lin− HSPCs (4×10^4 cells/mouse). DT treatment (50 μg/kg mouse) or mock treatment was given intraperitoneally every other day from day 0. *In vivo* imaging of the skull BMs of the recipients were taken on day 11.

In vivo antibody treatment

Non-irradiated BALB/c mice were transplanted with DiD-labelled B6 KSL HSPCs. On day 0 and day 2, rat anti-CD25 antibody (1 mg/mouse, PC-61, Bio X Cell) or control rat IgG antibody (1 mg/mouse, Bio X Cell) was given intravenously. Mouse anti-IL-10R antibody, anti-TGF-β antibody or control IgG antibody treatment (200 μg/mouse, Bio X Cell) was given intraperitoneally every other day from day −1 until day 7.

RNA Extraction and cDNA Synthesis

Isolated cells were homogenized using a 25-gauge syringe needle. Total RNA was extracted using Invitrogen's Purelink micro to midi kit (Carlsbad, CA) and the RNA concentration was measured on a Nanodrop ND 1000 spectrophotometer (Nanodrop, Wilmington, DE). 100ng of total RNA was converted into cDNA using Taqman Reverse Transcription kit (Applied Biosystems, Carlsbad, CA)[19].

Quantitative TaqMan Real-Time PCR

The ABI PRISM 7900HT Sequence Detection System was used for qt-RT-PCR analysis. All primer-probe (P&P) sets were custom designed. Custom designed P&P sets were validated by serially diluting cDNA isolated from cells expressing the target and verifying the slope, and by sequencing the amplicon. Taqman Fast PCR Master Mix was purchased from Qiagen (Valencia, CA). Amplification was carried out in a total volume of 25 μl for 40 cycles of 3 seconds at 95°C, 30 seconds at 60°C. Initial denaturation was performed for 3 min at 95°C. Target gene expression was normalized by total RNA quantity used for cDNA synthesis.

Immune reconstitution in RAG2 KO mice

CD4+CD25− cells and CD4+CD25+ cells were isolated from B6 mice and B6 IL-10 KO mice. B6 RAG2 KO mice were adoptively transferred with B6 wt CD4+CD25− T cells (1.5 million/mouse) and B6 IL-10 KO CD4+CD25+ Tregs (0.5 million/mouse), or wt CD4+CD25− T cells (1.5 million/mouse) and B6 CD4+CD25+ Tregs (0.5 million/mouse). One day later, DiD labelled BALB/c CD150+CD48−Lin− HSPCs were transplanted.

Supplementary Material

Refer to Web version on PubMed Central for supplementary material.

Acknowledgments

This work was supported by Bullock fellowship (to J.F.), the Harvard Stem Cell Institute and DoD W81XWH-10-1-0217 (to J.F. and C.P.L.), NIH HL097748 (to C.P.L), HL97794 (to D.T.S.), CA111519 (to M.S.), AI041521 (to T.B.S), EMBO (to C.L.C), HFSP (to C.L.C), philanthropic sources (to D.T.S. and C.L.C.), and the National Institutes of Health. We acknowlege Dr. Jie Zhao and Danny Cao at Photopathology Core of Wellman Center for Photomedicine of MGH for sorting.

References

1. Fuchs E, Tumbar T, Guasch G. Socializing with the neighbors: stem cells and their niche. Cell. 2004; 116(6):769–778. [PubMed: 15035980]
2. Li L, Xie T. Stem cell niche: structure and function. Annu Rev Cell Dev Biol. 2005; 21:605–631. [PubMed: 16212509]
3. Arai F, et al. Tie2/angiopoietin-1 signaling regulates hematopoietic stem cell quiescence in the bone marrow niche. Cell. 2004; 118(2):149–161. [PubMed: 15260986]
4. Niederkorn JY. See no evil, hear no evil, do no evil: the lessons of immune privilege. Nat Immunol. 2006; 7(4):354–359. [PubMed: 16550198]
5. Adams GB, Scadden DT. The hematopoietic stem cell in its place. Nat Immunol. 2006; 7(4):333–337. [PubMed: 16550195]
6. Zhang J, et al. Identification of the haematopoietic stem cell niche and control of the niche size. Nature. 2003; 425(6960):836–841. [PubMed: 14574412]
7. Calvi LM, et al. Osteoblastic cells regulate the haematopoietic stem cell niche. Nature. 2003; 425(6960):841–846. [PubMed: 14574413]
8. Feuerer M, et al. Bone marrow as a priming site for T-cell responses to blood-borne antigen. Nat Med. 2003; 9(9):1151–1157. [PubMed: 12910264]
9. Joffre O, et al. Prevention of acute and chronic allograft rejection with CD4+CD25+Foxp3+ regulatory T lymphocytes. Nat Med. 2008; 14(1):88–92. [PubMed: 18066074]
10. Zou L, et al. Bone marrow is a reservoir for CD4+CD25+ regulatory T cells that traffic through CXCL12/CXCR4 signals. Cancer Res. 2004; 64(22):8451–8455. [PubMed: 15548717]
11. Mazo IB, et al. Hematopoietic progenitor cell rolling in bone marrow microvessels: parallel contributions by endothelial selectins and vascular cell adhesion molecule 1. J Exp Med. 1998; 188(3):465–474. [PubMed: 9687524]
12. Celso CL, et al. Live-animal tracking of individual haematopoietic stem/progenitor cells in their niche. Nature. 2009; 457(7225):92–6. [PubMed: 19052546]
13. Sipkins DA, et al. In vivo imaging of specialized bone marrow endothelial microdomains for tumour engraftment. Nature. 2005; 435(7044):969–973. [PubMed: 15959517]
14. Huang Y, et al. Matching at the MHC class I K locus is essential for long-term engraftment of purified hematopoietic stem cells: a role for host NK cells in regulating HSC engraftment. Blood. 2004; 104(3):873–880. [PubMed: 15054040]
15. Jung Y, et al. Regulation of SDF-1 (CXCL12) production by osteoblasts; a possible mechanism for stem cell homing. Bone. 2006; 38(4):497–508. [PubMed: 16337237]
16. Sugiyama T, Kohara H, Noda M, Nagasawa T. Maintenance of the hematopoietic stem cell pool by CXCL12-CXCR4 chemokine signaling in bone marrow stromal cell niches. Immunity. 2006; 25(6):977–988. [PubMed: 17174120]
17. Mendez-Ferrer S, et al. Mesenchymal and haematopoietic stem cells form a unique bone marrow niche. Nature. 466(7308):829–834. [PubMed: 20703299]
18. Welniak LA, Blazar BR, Murphy WJ. Immunobiology of allogeneic hematopoietic stem cell transplantation. Annu Rev Immunol. 2007; 25:139–170. [PubMed: 17129175]
19. Bustin SA. Absolute quantification of mRNA using real-time reverse transcription polymerase chain reaction assays. J Mol Endocrinol. 2000; 25(2):169–193. [PubMed: 11013345]

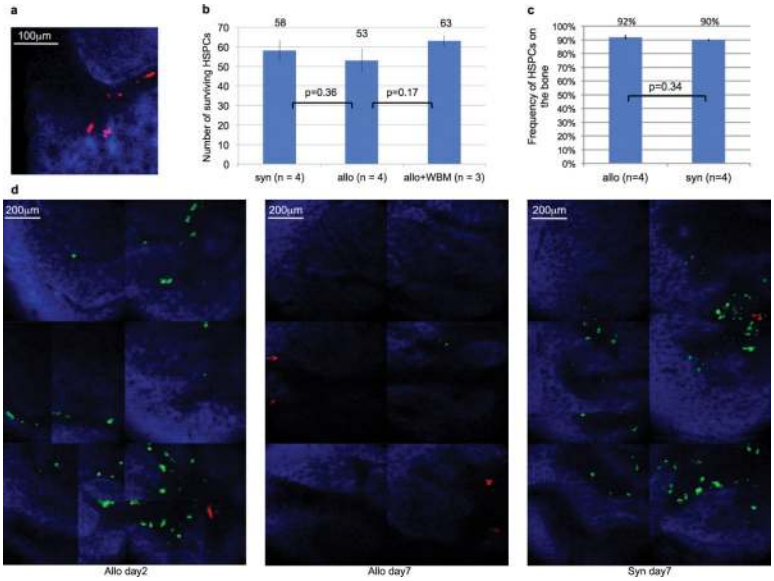

Figure 1. Allo-HSPCs survive without IS for 30 days

a, *In vivo* imaging of DiD-labelled B6 KSL HSPCs (red) surviving on the endosteal surface of the skull BM of BALB/c recipients for 30 days without IS. Blue; Bone. Black area is BM cavity.

b, Comparable numbers of DiD-labelled B6 KSL HSPCs (5×10^4 cells/mouse) in the skull BM on day 30 after transplantation into B6 (Syn) mice or BALB/c (Allo) mice (n=4 recipients). Co-transplantation of non-labelled B6 whole bone marrow (WBM) cells did not affect the number of surviving HSPCs (n=3 recipients). Cell numbers were counted in identical volumes of the skull covering 1650 μm in x, 2310 μm in y, and 150 μm in z. Error bar indicates standard error.

c, Majority of B6 donor KSL cells localize within 15 μm of the endosteal surface both in B6 and BALB/c recipients on day 30 after transplantation. Error bar indicates standard error (n=4).

d, Montage pictures of the skull BMs of non-irradiated BALB/c mice or B6 mice 7 days after transplantation of DiD-labelled B6 KSL HSPCs (red) and DiI-labelled B6 Lin+ differentiated cells (green). Blue; Bone. Black area is BM cavity. Image size was 880 μm (x) × 1320 μm (y) around the coronal sutures and central vein.

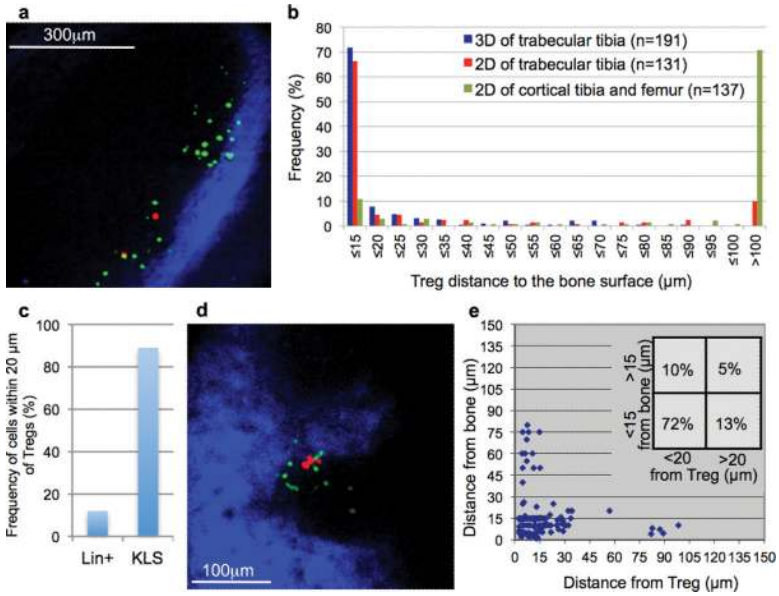

Figure 2. FoxP3 Tregs accumulate on endosteal surface, form clusters around adoptively transferred HSPCs and around allo-HSPCs that survive after 30 days

a, *In vivo* imaging of the tibia trabecular BM of B6 FoxP3−GFP mice transplanted with DiD-labelled B6 KSL HSPCs. FoxP3−GFP Tregs (green) accumulate on the endosteal surface. 81% (83/103) of DiD-labelled B6 KSL HSPCs (red) home within 20 μm of Tregs. Blue; bone. Black area is BM cavity. The maximal imaging depth of the tibia trabecular BM was approximately 150 μm below the bone surface, while the size of the tibia BM space confined by anastomosing trabeculae ranged between 50-250 μm based on the micro-computed tomography analysis (data not shown).

b, Histogram depicting the distance of FoxP3−GFP Tregs to the endosteal surface. 3D results were obtained by IVM, while 2D results were obtained from histological sections.

c, Frequency of adoptively transferred KSL cells (89% (338/380)) and Lin+ cells (12% (42/330)) homing within 20 μm of FoxP3−GFP Tregs in the skull BM.

d, *In vivo* imaging of 5-FU resistant DiD-labelled KSL HSPCs (red) forming clusters with FoxP3 Tregs (green) on the endosteal surface. Blue; bone. Black area is BM cavity.

e, Spatial distribution of B6 KSL HSPCs surviving in the skull BM of non-irradiated BALB/c FoxP3−GFP mice for 30 days relative to the endosteal surface and Tregs. Measurements were taken from 3D *in vivo* skull BM image stacks.

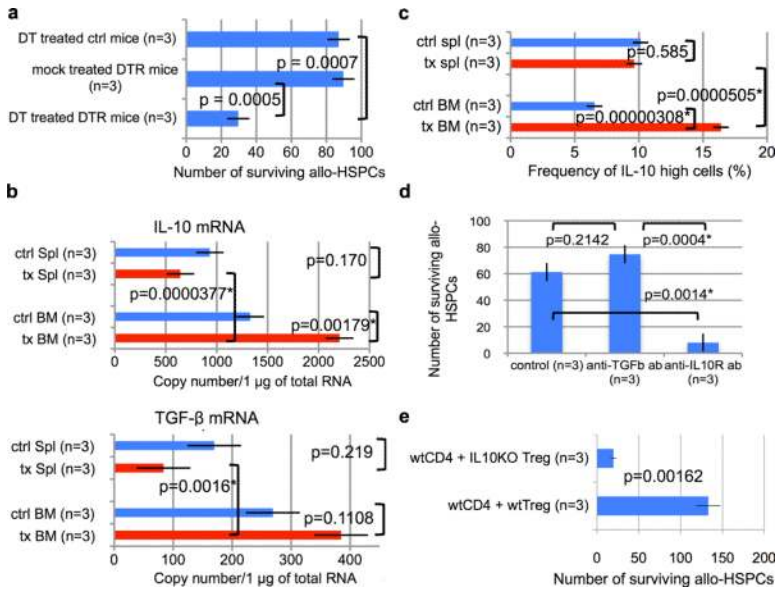

Figure 3. BM Tregs are critical in suppressing the rejection of allo-HSPCs in immune competent recipients in an IL-10 dependent manner

a, The number of DiD-labelled BALB/c CD150+CD48−Lin− HSPCs in the skull BM of DT treated FoxP3−GFP DTR mice (B6N9), mock treated FoxP3−GFP DTR mice (B6N9), and DT treated control mice (B6N9). Cells were counted in identical volumes 2640 μm (x) × 3330 μm (y) × 150 μm (z) in size. Error bar indicates standard error (n=3).

b, Qt-RT-PCR analysis of FoxP3+ Tregs isolated from B6 FoxP3−GFP recipients 6 days after transplantation of BALB/c CD150+CD48−Lin− HSPCs without IS. Results are expressed as copy number/1 μg of total RNA. Error bars indicate standard error (n=3).

c, Intracellular staining of IL-10 in FoxP3−GFP Tregs in non-irradiated mice with and without allo-HSPC transplants. Error bar indicates standard error (n=3).

d, Quantification of DiD-labelled B6 KSL cells in the skull BM of anti-IL-10R, anti-TGF-β or control IgG antibody treated BALB/c mice after transplantation of DiD-labelled B6 KSL cells without IS. Error bar indicates standard error (n=3). Cells were counted in identical volumes 2620 μm (x) × 2200 μm (y) × 150 μm (z) in size.

e, Quantification of DiD-labelled BALB/c CD150+CD48−Lin− HSPCs in the skull BM of B6 RAG2 KO mice reconstituted with wt CD4+CD25− T cells and IL-10 KO CD4+CD25+ Tregs or with wt CD4+CD25− T cells and wt CD4+CD25+ Tregs. Cells were counted in identical volumes 2640 μm (x) × 3330 μm (y) × 150 μm (z) in size. Error bar indicates standard error (n=3).